Maximum Efficiency Control on the Receiving Side Using LCC-LCC Compensation Topology for Dynamic Wireless Power Transfer

Koshi Ikeda
Faculty of Science and Technolog
Tokyo University of Science
Noda, Japan
7322509@ed.tus.ac.jp

Takehiro Imura
Faculty of Science and Technology
Tokyo University of Science
Noda, Japan

Yoichi Hori
Faculty of Science and Technology
Tokyo University of Science
Noda, Japan

***Abstract*— Transmission efficiency is one of the most important characteristics in dynamic wireless power transfer for battery electric vehicles. In this paper, the LCC-LCC compensation topology, which does not require complicated control in a transmission system, is used as the compensation topology. To facilitate laying and maintenance, the transmission system should be as simple as possible in configuration and control. On the other hand, there is no problem even if the receiving side uses a slightly more complicated control than the transmission side. Therefore, on the receiving side, a coupling coefficient is estimated in real time from the voltage and current values measured between the rectifier and the DC/DC converter. Then, maximum efficiency control is achieved by updating the duty ratio of the DC/DC converter to follow the optimum load. The effectiveness of the proposed method was demonstrated through the simulations and experiments.**

Keywords—Battery electric vehicle, Dynamic wireless power transfer, LCC-LCC compensation topology, Coupling coefficient estimation, Maximum efficiency control

I. INTRODUCTION

In recent years, battery electric vehicles (BEVs) have been attracting attention from the viewpoint of environmental issues. However, the drawbacks of BEVs are their short cruising range, long charging time and lack of charging spots. One of the solutions to these problems is the dynamic wireless power transfer (DWPT) [1][2]. The power transmission circuits of DWPT include the S-S (Series-Series) compensation topology and the LCC-LCC compensation topology that incorporates LCL filters with gyrator characteristics [3][4]. The S-S compensation topology is a common circuit in the DWPT, but it is subject to an AC short-circuit state in which large current flows from the power supply when there is no vehicle on the transmission coil, i.e., when the coupling coefficient is zero. On the other hand, there is no danger of an AC short-circuit condition in the LCC-LCC compensation topology. In addition, control is important for DWPT, where system conditions are constantly changing, to improve safety and efficiency. There are various maximum efficiency controls for circuits other than the LCC-LCC compensation topology [5]-[7]. However, a system that simulates battery charging while controlling maximum efficiency through coupling coefficient estimation has not yet been proposed for the LCC-LCC compensation topology. The transmission side of the DWPT system must be easy to install and maintain, so it is necessary to use a simple configuration and control. Therefore, in this paper, a method to maximize the transmission efficiency using the LCC-LCC compensation topology, which does not require coil switching control and has the advantage that multiple transmission circuits can be connected to a single inverter is proposed. In order to confirm the usefulness of the proposed method, simulations and experiments are conducted.

II. WIRELESS POWER TRANSFER FOR LCC-LCC COMPENSATION TOPOLOGY

This chapter presents the circuit configuration used in the proposed method and its characteristics. Fig.1 shows the schematic of the LCC-LCC compensation topology. The input voltage is represented by v_1, the output voltage by v_2, the inductance of the transmitting and receiving coils by L_T and L_R, the capacitance of the resonance by C_{Tp},C_{Ts}, C_{Rs} and C_{Rp}, the inductance of the resonance by L_{T0} and L_{R0}, the mutual inductance by L_m and the load by R_L. The LCC-LCC compensation topology has LCC filters with gyrator characteristics as compensation circuits. By inserting C_{Tp}, it has the effect of reducing the value of L_{T0} and increasing the transmission power. The inductance and capacitance satisfy the resonance condition (1) shown below with the angular frequency ω_0. Mutual inductance L_m can be expressed by (2) using the coupling coefficient k, so the current I_{in} flowing from the power supply is shown in (3). From (3), when the coupling coefficient k between the transmitting coil and the receiving coil is 0, the current I_{in} flowing from the power supply is 0 and the closed loop L_T including the transmitting coil is in an antiresonance state. Therefore, the LCC-LCC compensation topology is considered practical as it does not draw excessive current even if the system malfunctions.

$$\omega_0 = \frac{1}{\sqrt{L_{T0}C_{Tp}}} = \sqrt{\frac{C_{Tp}+C_{Ts}}{L_T C_{Tp} C_{Ts}}} = \frac{1}{\sqrt{L_{R0}C_{Rp}}} = \sqrt{\frac{C_{Rp}+C_{Rs}}{L_R C_{Rp} C_{Rs}}} \quad (1)$$

$$L_m = k\sqrt{L_T L_R} \quad (2)$$

$$I_{in} = {\omega_0}^3 C_{Tp} C_{Rp} k \sqrt{L_T L_R} V_2 \quad (3)$$

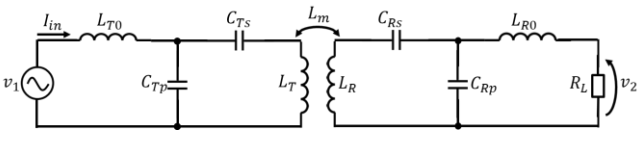

Fig. 1. The LCC-LCC compensation topology.

III. Calculation of Maximum Efficiency Point

In order to obtain the maximum efficiency point in the DWPT, a simple model is used to derive the equation. Fig.2 shows the equivalent circuit of the LCC-LCC compensation topology with a constant voltage.

In Fig.2, R_L indicates the equivalent load resistance in the LCC-LCC compensation topology. The internal resistance of each inductor is represented by R_T, R_R, R_{T0} and R_{R0}. The transmission efficiency η in the LCC-LCC compensation topology is shown in (4).

$$\eta = \frac{{\omega_0}^2 k^2 L_T L_R R_L}{\left\{(R_{R0}+R_L)A_4+\frac{A_1}{{\omega_0}^2 {C_{Rp}}^2}\right\}\left\{(R_{R0}+R_L)A_3+\frac{R_T}{{\omega_0}^2 {C_{Rp}}^2}\right\}}$$

$$A_1 = {\omega_0}^2 R_{T0} R_T {C_{Tp}}^2 + 1$$

$$A_2 = {\omega_0}^4 R_{T0} k^2 L_T L_R {C_{Tp}}^2$$

$$A_3 = R_T R_R + {\omega_0}^2 k^2 L_T L_R$$

$$A_4 = R_R A_1 + A_2 \tag{4}$$

From (4), the transmission efficiency η depends on the equivalent load resistance R_L in the WPT. Therefore, by differentiating the transmission efficiency η with respect to R_L, the point $R_{L\eta max}$ at which the efficiency is maximized at R_L is shown in (5).

$$R_{L\eta max} = \frac{1}{{\omega_0}^2 {C_{Rp}}^2}\sqrt{\frac{R_T A_1}{A_3 A_4}} \tag{5}$$

Maximum efficiency of the system can be achieved if the equivalent load resistance can be varied according to (5). However, it is difficult to directly manipulate the equivalent load resistance on the receiving side. When considering the WPT to BEVs, the load is a constant voltage load such as a battery or capacitor after rectification, so the DC/DC converter is placed in front of the constant voltage load to control the receiving side voltage. Equation (6) shows the relationship between the equivalent load resistance R_L and the receiving side voltage V_2 derived from Fig.2 and the receiving side voltage that maximizes transmission efficiency $V_{2\eta max}$ from (5).

Deriving the relationship between the equivalent load resistance R_L and the receiving side voltage V_2 from Fig.2 and using (5) to formulate the receiving side voltage that maximizes the efficiency $V_{2\eta max}$, (6) can be obtained.

$$V_{2\eta max} = \frac{\omega_0 k \sqrt{L_T L_R}\frac{C_{Tp}}{C_{Rp}} V_1}{A_4\left\{{\omega_0}^2 R_{R0} {C_{Rp}}^2 \sqrt{\frac{A_3 A_4}{R_T A_1}}-1\right\}+\sqrt{\frac{A_1 A_3 A_4}{R_T}}} \tag{6}$$

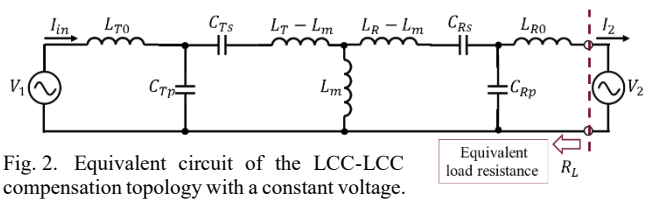

Fig. 2. Equivalent circuit of the LCC-LCC compensation topology with a constant voltage.

IV. Estimation of Coupling Coefficient

A. Derivation of coupling coefficient

In maximum efficiency control, the DC/DC converter is controlled using $V_{2\eta max}$ as the command value. However, information on the coupling coefficient k is necessary to calculate $V_{2\eta max}$ from (6). In this paper, a method of estimating the coupling coefficient k by sensing only the voltage and current on the receiving side without using information on the voltage and current that change on the transmission side. As a precondition, the transmission side voltage V_1 is standardized to a constant voltage for each road, and V_1, L_{T0} and L_T are known information and can be obtained in advance. Deriving the receiving side current I_2 from Fig.2 and converting it to the coupling coefficient k can be expressed as (7). Here (7) has two solutions, but since k is positive, only the solution with positive sign is used.

$$k = \frac{-V_1 \pm \sqrt{{V_1}^2 - 4R_{T0}A_{k1}\{(A_1-1)A_{k1}A_{k3}-(A_1+R_{R0}A_{k2})I_2+A_{k2}V_2\}}}{2{\omega_0}^3 R_{T0}\sqrt{L_T L_R}C_{Tp}C_{Rp}A_{k1}}$$

$$A_{k1} = V_2 - R_{R0} I_2$$

$$A_{k2} = {\omega_0}^2 R_R {C_{Tp}}^2 \tag{7}$$

B. Noise reduction in coupling coefficent estimation

Considering the introduction to an actual system, noise always occurs in the measured values read from the voltage/current sensors used for coupling coefficient estimation. In the proposed control method, (7) is used to update the command value of the duty ratio of the DC/DC converter, so it is necessary to reduce the influence of noise as much as possible. Hence, the coupling coefficient is estimated using the method of statistically correcting the estimated value by the recursive least squares filter. Outputs $y[i]$ and regressor $\varphi[i]$ are defined as in (8) and (9), where i is represents a sampling point.

$$y[i] = -V_1 + \sqrt{{V_1}^2 - 4R_{T0}A_{k1}\{(A_1-1)A_{k1}A_{k3}-(A_1+R_{R0}A_{k2})I_2+A_{k2}V_2\}} \tag{8}$$

$$\varphi[i] = 2{\omega_0}^3 R_{T0}\sqrt{L_T L_R}C_{Tp}C_{Rp}A_{k1} \tag{9}$$

The estimated values of the coupling coefficient $\hat{k}[i]$, $y[i]$ and $\varphi[i]$ are successively updated according to the algorithms shown in (10) to (12). Where, λ is an oblivion coefficient, $\hat{k}[0] = 0$ and $P[0] = 0$.

$$\hat{k}[i] = \hat{k}[i-1] + \frac{\varphi[i]P[i-1]}{\lambda+\varphi[i]^2 P[i-1]}\epsilon[i] \tag{10}$$

$$\epsilon[i] = y[i] - \varphi[i]\hat{k}[i-1] \tag{11}$$

$$P[i] = \frac{1}{\lambda}\left\{P[i-1] - \frac{\varphi[i]^2 P[i-1]^2}{\lambda+\varphi[i]^2 P[i-1]}\right\} \tag{12}$$

V. Conversion to DC Value

In (6) and (7), effective values such as V_1, V_2 and I_2 were used to simplify the derivation. However, since the inverter shown in Fig.3 is driven at 85 kHz, the transmission side voltage and the receiving side voltage become rectangular waves, which cannot be used for control as they are.

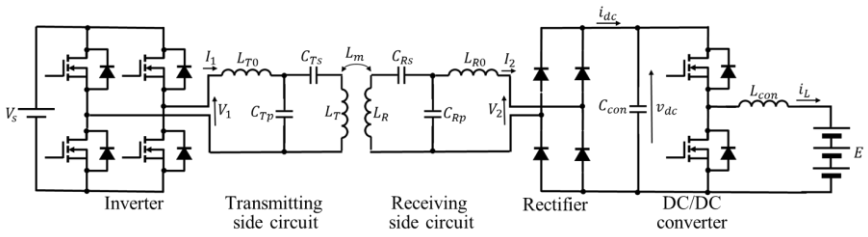

Fig. 3. Overall circuit configuration including transmitting and receiving side circuit.

Also, considering the measurement with the sensor, it is easier to measure the DC portion than the AC portion. Therefore, the average value of i_{dc} in Fig.3, $\overline{i_{dc}}$ and v_{dc} are used to converter the AC values to the DC values. As described above, since the transmission side voltage is a rectangular wave, using Fourier series expansion, the effective value V_1 of the fundamental wave component of the transmission side voltage can be expressed as (13) using V_s. Similarly, the fundamental wave component effective value V_2 of the receiving side voltage can be expressed as in (13) using the smoothing capacitor voltage v_{dc}. Since the receiving side current is the sine wave, I_2 can be expressed as in (13) using $\overline{i_{dc}}$ from the relationship between the average value and the effective value of the sine wave. Using (13), $V_{2\eta max}$ shown in (6) can be rewritten as $v_{dc\eta max}$ shown in (14). Also, (7) indicating the coupling coefficient k can be expressed as (15).

$$V_1 = \frac{2\sqrt{2}}{\pi} V_s \ , \ V_2 = \frac{2\sqrt{2}}{\pi} v_{dc} \ , \ I_2 = \frac{\pi}{2\sqrt{2}} \overline{i_{dc}} \tag{13}$$

$$v_{dc\eta max} = \frac{\omega_0 k \sqrt{L_T L_R} \frac{C_{Tp}}{C_{Rp}} V_s}{A_4 \left\{ {\omega_0}^2 R_{R0} {C_{Rp}}^2 \sqrt{\frac{A_3 A_4}{R_T A_1}} - 1 \right\} + \sqrt{\frac{A_1 A_3 A_4}{R_T}}} \tag{14}$$

$$k = \frac{-8V_s + \sqrt{64{V_1}^2 - 4R_{T0}A_{k1dc}\{(A_1-1)A_{k1dc}A_{k3} - \pi^2(A_1 + R_{R0}A_{k2})I_2 + 8A_{k2}V_2\}}}{2{\omega_0}^3 R_{T0}\sqrt{L_T L_R} C_{Tp} C_{Rp} A_{k1}}$$

$$A_{k1dc} = 8V_{dc} - \pi^2 R_{R0} \overline{i_{dc}} \tag{15}$$

VI. Controlled by DC/DC converter

In the DC/DC converter shown in Fig.3, C_{con} is the smoothing capacitor after the rectifier, L_{con} is the inductor after the DC/DC converter, E is the battery voltage, and i_L is the current flowing into the battery. Also, let R_{con} be the sum of the internal resistances of the inductor and the battery. In the proposed system, i_{dc} has the full-wave rectified waveform, but the frequency used for DWPT is 85 kHz, which is sufficiently higher than the switching frequency of the DC/DC converter. Hence, i_{dc} can be treated as the average value, denoted as $\overline{i_{dc}}$.

A. Modeling by state averaging method

In this section, the DC/DC converter is modeled using the state averaging method. The two switches of the DC/DC converter in Fig.3 operate reciprocally. $d(t)$ is defined as the ON time duty ratio of the upper side switch. The state averaging method is a method of formulating circuit equations for the two states when the upper side switch is ON and OFF, and averaging them weighted by the duty ratio. Modeling the DC/DC converter by the state averaging method yields (16) and (17).

$$\frac{d}{dt}\begin{bmatrix} i_L(t) \\ v_{dc}(t) \end{bmatrix} = \begin{bmatrix} -\frac{R_{con}}{L_{con}} & \frac{d(t)}{L} \\ -\frac{d(t)}{C_{con}} & 0 \end{bmatrix} \begin{bmatrix} i_L(t) \\ v_{dc}(t) \end{bmatrix} + \begin{bmatrix} -\frac{1}{L_{con}} & 0 \\ 0 & \frac{1}{C_{con}} \end{bmatrix} \begin{bmatrix} E \\ \overline{i_{dc}}(t) \end{bmatrix} \tag{16}$$

$$v_{dc}(t) = \begin{bmatrix} 0 & 1 \end{bmatrix} \begin{bmatrix} i_L(t) \\ v_{dc}(t) \end{bmatrix} \tag{17}$$

However, this model is a nonlinear model. Therefore, to apply linear control theory, linearization is performed by dividing the equilibrium point and the minute fluctuations around the equilibrium point. The equilibrium points of $d(t)$, $i_L(t)$, $v_{dc}(t)$ and $\overline{i_{dc}}(t)$ are respectively denoted by D, I_L, V_{dc} and $\overline{I_{dc}}$, and the minute fluctuations around the equilibrium points are respectively denoted by $\Delta d(t)$, $\Delta i_L(t)$, $\Delta v_{dc}(t)$ and $\Delta\overline{i_{dc}}(t)$. Linearizing the model of (16) and (17) yields (18) and (19). Also, from (16) and (17), the equilibrium point of this satisfies (20) and (21).

$$\frac{d}{dt}\begin{bmatrix} \Delta i_L(t) \\ \Delta v_{dc}(t) \end{bmatrix} = \begin{bmatrix} -\frac{R_{con}}{L_{con}} & \frac{D}{L} \\ -\frac{D}{C_{con}} & 0 \end{bmatrix} \begin{bmatrix} \Delta i_L(t) \\ \Delta v_{dc}(t) \end{bmatrix} + \begin{bmatrix} \frac{V_{dc}}{L_{con}} & 0 \\ -\frac{I_L}{C_{con}} & \frac{1}{C_{con}} \end{bmatrix} \begin{bmatrix} \Delta d(t) \\ \Delta\overline{i_{dc}}(t) \end{bmatrix} \tag{18}$$

$$\Delta v_{dc}(t) = \begin{bmatrix} 0 & 1 \end{bmatrix} \begin{bmatrix} \Delta i_L(t) \\ \Delta v_{dc}(t) \end{bmatrix} \tag{19}$$

$$V_{dc} = \frac{ED + R_{con}\overline{I_{dc}}}{D^2} \tag{20}$$

$$I_L = \frac{\overline{I_{dc}}}{D} \tag{21}$$

Furthermore, as can be seen from Fig.3, $\overline{I_{dc}}$ is determined by the convenience of the power transmission side, and is expressed as (22). Using (20) and the state equations expressed by (18) and (19), the state equation of the small-signal model around the equilibrium point is obtained.

$$\overline{I_{dc}} = \frac{8}{\pi^2} \frac{{\omega_0}^3 k \sqrt{L_T L_R} C_{1p} C_{2p} V_s + {\omega_0}^2 {C_{Rp}}^2 (R_R A_1 + A_2) V_{dc}}{{\omega_0}^2 R_{R0} {C_{Rp}}^2 A_4 + A_1} \tag{22}$$

B. Duty ratio, which is the command value for control

From (20) to (22), the command value for the duty ratio D of the upper side switch that gives the equilibrium point when performing maximum efficiency control is given by (23). Where $\overline{I_{dc(v_{dc\eta max})}}$ is obtained by substituting $v_{dc\eta max}$ for $\overline{I_{dc}}$ in (22).

$$D = \frac{E \pm \sqrt{E^2 + 4R_{con} v_{dc\eta max} \overline{I_{dc(v_{dc\eta max})}}}}{2 v_{dc\eta max}} \tag{23}$$

In (23), there are two solutions for D, but $0 < D < 1$ and the solution with the larger value is used. Also, the transfer function from $\Delta d(s)$ to $\Delta v_{dc}(s)$ is obtained as shown in (24) from the Laplace transform of the state equation.

$$\frac{\Delta v_{dc}(s)}{\Delta d(s)} = \frac{b_1 s + b_0}{s^2 + a_1 s + a_0} \tag{24}$$

$$a_1 = \frac{R_{con}}{L_{con}} - \frac{8}{\pi^2} \frac{{\omega_0}^2 {C_{Rp}}^2 (R_R A_1 + A_2)}{C_{con}\{{\omega_0}^2 R_{R0} {C_{Rp}}^2 (R_R A_1 + A_2) + A_1\}}$$

$$a_0 = \frac{1}{L_{con} C_{con}} \left\{ D^2 - \frac{8}{\pi^2} \frac{{\omega_0}^2 R_{con} {C_{Rp}}^2 (R_R A_1 + A_2)}{\{{\omega_0}^2 R_{R0} {C_{Rp}}^2 (R_R A_1 + A_2) + A_1\}} \right\}$$

$$b_1 = -\frac{I_L}{C_{con}} \ , \ b_0 = -\frac{R_{con} I_L + D V_{dc}}{L_{con} C_{con}}$$

C. *Feedback system design by pole placement method*

The pole placement method is a control method that regards the controller that performs PID control and the controlled object as a single transfer function. By moving the pole of the transfer function to an arbitrary position, the objects is controlled to a stable as quickly as possible. In this paper, since (24) is a second-order transfer function, by designing the PID controller shown in (25) using the pole placement method, a feedback system of $\Delta v_{dc}(s)$ are designed with a pole ω_c at the arbitrary position. In (25), K_P, K_I and K_D are the coefficients of the PID controller, and a_{c1}, b_{c0}, b_{c1} and b_{c2} are used as the coefficients when expressing these in a more organized form. Here, the transfer function from the target value $v_{dc\eta max}(s)$ to the controlled variable $v_{dc}(s)$ is given by (26). Where $\Delta P_v(s)$ is the plant model of the DC/DC converter, which is the object to be controlled, and here refers to $\frac{\Delta v_{dc}(s)}{\Delta d(s)}$.

$$C_{PID}(s) = K_P + \frac{K_I}{s} + \frac{K_D s}{\tau s + 1} = \frac{b_{c2} s^2 + b_{c1} s + b_{c0}}{s^2 + a_{c1} s} \tag{25}$$

$$\frac{v_{dc}(s)}{v_{dc\eta max}(s)} = \frac{C_{PID}(s) \Delta P_v(s)}{1 + C_{PID}(s) \Delta P_v(s)} \tag{26}$$

When (26) is rearranged, the denominator becomes a fourth-degree polynomial. The pole placement method is designed so that the fourth-order polynomial in the denominator of (26) and $(s + \omega_c)^4$, which has a quadruple root at the pole ω_c, are the same. The Sylvester matrix for determining whether two polynomials have a common root is represented by (27). By solving this matrix for a_{c1}, b_{c0}, b_{c1} and b_{c2}, it is possible to perform feedback control with poles always at the set positions.

$$\begin{bmatrix} 1 & 0 & 0 & 0 & 0 \\ a_1 & 1 & b_1 & 0 & 0 \\ a_0 & a_1 & b_0 & b_1 & 0 \\ 0 & a_0 & 0 & b_0 & b_1 \\ 0 & 0 & 0 & 0 & b_0 \end{bmatrix} \begin{bmatrix} 1 \\ a_{c1} \\ b_{c2} \\ b_{c1} \\ b_{c0} \end{bmatrix} = \begin{bmatrix} 1 \\ 4\omega_c \\ 6{\omega_c}^2 \\ 4{\omega_c}^3 \\ {\omega_c}^4 \end{bmatrix} \tag{27}$$

Fig.4 shows a block diagram showing the flow from coupling coefficient estimation to maximum efficiency control. The coupling coefficient k is estimated from v_{dc} and i_{dc} measured by the sensor. Next, calculate the smoothing capacitor voltage $v_{dc\eta max}$ that provides the maximum efficiency, and obtained and output D shown in (23). Furthermore, the transfer function of the small-signal model of the DC/DC converter is updated in real time from (24), each coefficient is calculated form (27), and Δd is output.

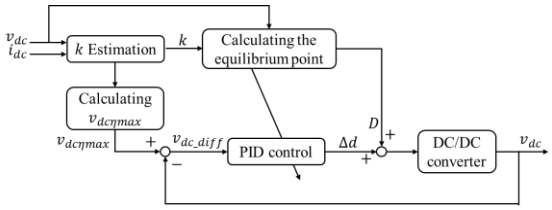

Fig. 4. Block diagram showing control flow.

VII. Simulations and Experiments

In this chapter, simulations and experimental results of the proposed "maximum efficiency control on the receiving side using LCC-LCC compensation topology for DWPT" are presented.

A. *Simulations and experimental conditions*

Table 1 shows the parameters used in the simulations and experiments. The duty ratio of the DC/DC converter stands by at $d(t) = 0.95$ when not receiving the power, and starts coupling coefficient estimation as soon as it senses the power. The oblivion coefficient λ of the recursive least squares filter was set to 0.95, and all the poles of the feedback loop were arranged as quadruple roots at $\omega_c = -2\pi \times 1000$ rad/s. The sensor sampling period is 50 μs. The size of the transmitting side coil is 250 mm × 500 mm, and the size of receiving side coil is 250 mm × 250 mm. DWPT was simulated by moving the receiving side coil at 20 km/h in the simulations and 3.6 km/h in the experiments. Fig.5 shows the positional relationship of the coils in the simulations. In addition, Fig.6 shows the state and equipment of the experiments.

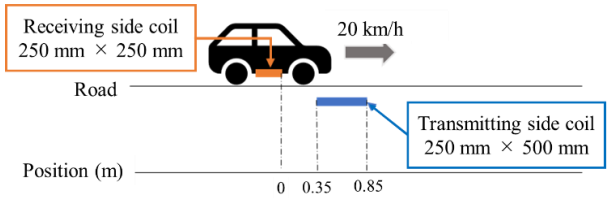

Fig. 5. Conditions of simulations.

TABLE I. PARAMETERS USED IN SIMULATIONS AND EXPERIMENTS

Parameter	Value	
	Transmitting side	Receiving side
Inductance L_T, L_R [μH]	206.7	111.4
Resistance R_T, R_R [Ω]	0.30	0.15
Compensated capacitance C_{Ts}, C_{Rs} [nF]	22.35	56.36
Compensated inductance L_{T0}, L_{R0} [μH]	49.81	49.23
Compensated resistance R_{T0}, R_{R0} [Ω]	0.13	0.15
Compensated capacitance C_{Tp}, C_{Rp} [nF]	70.39	71.22
Operation frequency f_0 [kHz]	85	
Input voltage V_s [V]	20	
DC/DC converter frequency f_s [kHz]	10	
Smoothing capacitance C_{con} [μF]	11	
Battery voltage E [V]	10	
DC/DC converter frequency L_{con}[μH]	2180	
DC/DC converter frequency R_{con} [Ω]	0.72	

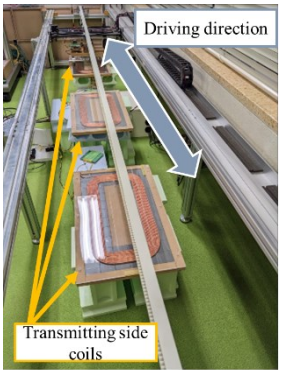

(a) DWPT simulator.

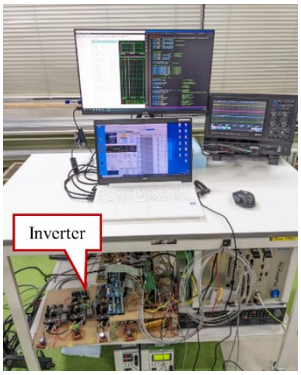

(b) State of experiments.

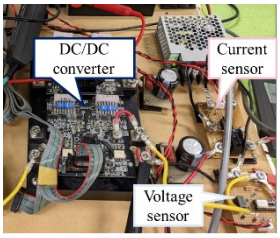

(c) DC/DC converter and sensors.

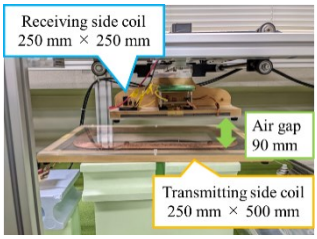

(d) Each Coil size and air gap.

Fig. 6. Experimental equipment.

B. *Simulation results*

Fig.7(a) shows the graph of coupling coefficients in the simulation. The red line shows the true value of the coupling coefficient k, and the blue line shows the graph obtained by k estimation. No significant delay in estimation was observed in the simulations. Since the coupling before and after the null point, which occurs at the beginning and the end of the power feed, affects the estimation of the coupling coefficients, a threshold value is set according to the current value. This indicates that the estimation is performed only between 0.06 s to 0.155 s. Although the estimated values of the coupling coefficients show a certain degree of followability, the estimated values have an error of 0.03 at the maximum with respect to the true values. This may be due to the fact that the coupling coefficients calculated in Chapter 4 were calculated using a model in which the voltage source is after the rectifier, without considering the effect of the DC/DC converter for the sake of simplicity.

Fig.7(b) shows the graph of the upper switching duty ratio $d(t)$ of the DC/DC converter and Fig.7(c) shows the graph of the smoothing capacitor voltage v_{dc}. The fact that $d(t)$ decreases to reach the maximum efficiency and v_{dc} increases accordingly indicates that the control is adaptive. Fig.7(d) also shows graphs of the transmission side power P_1 and the receiving side power P_2. Fig.7(e) and (f) show that the proposed maximum efficiency control improves the efficiency by about 10 % in all regions compared to the case without the control. The simulation results show the effectiveness of the proposed control method in the DWPT system.

C. *Experimental results*

In the experiments, DWPT was performed for three transmission circuits. Fig.8 shows the experimental results of the proposed maximum efficiency control. Fig.8(a) shows the graph of coupling coefficients. It can be seen that the estimated coupling coefficient shown by the blue line follows the true value of the coupling coefficient shown by the red line.

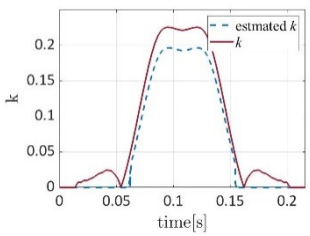

(a) k estimation.

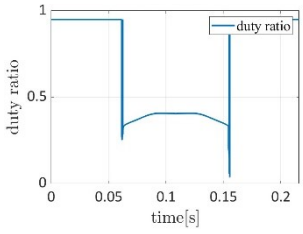

(b) Duty ratio.

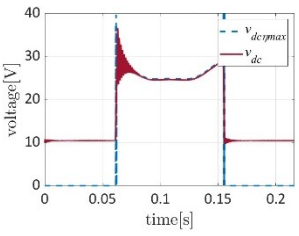

(c) Receiving side voltage.

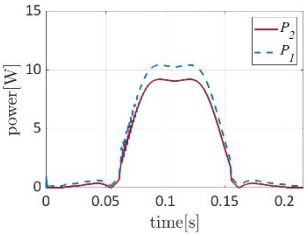

(d) Power.

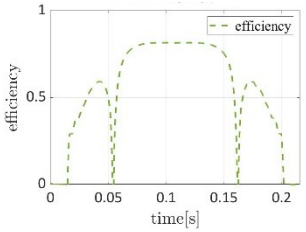

(e) Efficiency (without control).

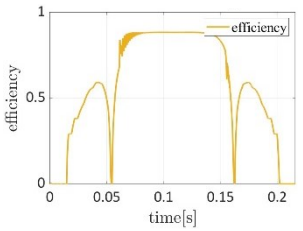

(f) Efficiency (with control).

Fig. 7. Results of maximum efficiency control and simulation results of efficiency withouot control.

This allowed the operability of the coupling coefficient estimation to be verified by experiment. Fig.8(b) shows graphs of the receiving side DC voltage v_{dc} in the red line, and the receiving side DC voltage $v_{dc\eta max}$ during maximum efficiency control in the blue dotted line. The comparison of the graphs of v_{dc} and $v_{dc\eta max}$ shows that the actual measured voltage value v_{dc} follows the voltage $v_{dc\eta max}$ that calculated at maximum efficiency control point, indicating that the DC/DC converter can be controlled according to the command value. Fig.8(c) shows the DC current on the transmission side of the blue line and the DC current on the receiving side of the red line. Fig.8(d) shows the duty ratio, Fig.8(e) shows the power transmitted on the blue line and the power received on the red line, and (f) shows the efficiency graph. From Fig.8(d) and (f), it can be seen that the efficiency can be kept above 80% in the power transmission section. To demonstrate the effectiveness of the proposed method, Fig.9 shows graphs for a constant duty ratio of 0.95, i.e., the voltage on the power receiving side is always kept constant around the battery voltage and no control is applied. Fig.9(a) to (c) show the graphs of duty ratio, power, and efficiency, respectively, and will be compared with Fig.8(d) to (f). From Fig.8(e) and Fig.9(b), the instantaneous power obtained is twice different with control. From Fig.8(f) and Fig.9(c), it can also be seen that the efficiency increased by about 10% with the control. Thus, the experimental results show the effectiveness of the proposed control method in the DWPT system. Although the efficiency is lower in the experiment than in the simulation, it is considered to be due to switching losses in the inverter and DC/DC converter and losses due to heat generation in the elements.

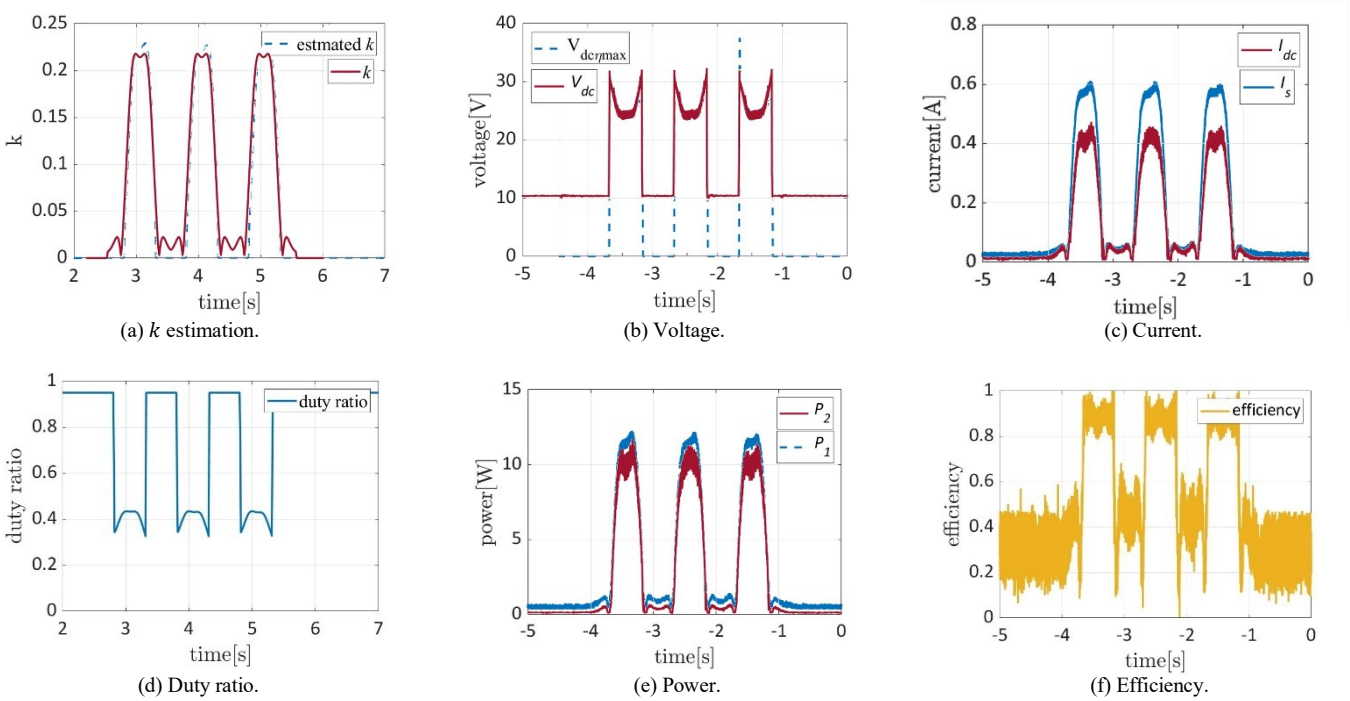

(a) k estimation. (b) Voltage. (c) Current.

(d) Duty ratio. (e) Power. (f) Efficiency.

Fig. 8. Experimental results of maximum efficiency control.

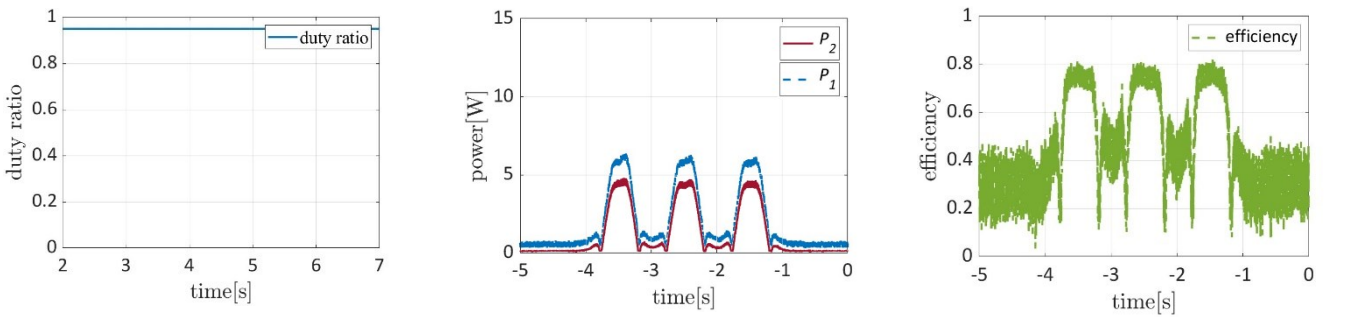

(a) Duty ratio. (b) Power. (c) Efficiency.

Fig. 9. Results of maximum efficiency control and simulation results of efficiency withouot control.

VIII. Conclusion

In this paper, a control method for DWPT systems was proposed to maximize transmission efficiency using the LCC-LCC compensation topology , which has the advantages of being safer than the S-S compensation topology and not requiring complex control on the transmission side. The maximum efficiency control was achieved in real-time by estimating the coupling coefficient using the known values of the circuit constants and the values measured only at the power receiving side. In addition, the simulation and experiments showed that the efficiency was increased when maximum efficiency control was performed compared to the case without control, demonstrating the effectiveness of the proposed method. Based on the above, future studies include kW-class experiments in a real environment to verify whether the system can actually be used in a car.

References

[1] A. C. Bagchi, A. Kamineni, R. A. Zane and R. Carlson, "Review and Comparative Analysis of Topologies and Control Methods in Dynamic Wireless Charging of Electric Vehicles," in IEEE Journal of Emerging and Selected Topics in Power Electronics, vol. 9, no. 4, pp. 4947-4962, Aug. 2021.

[2] A. N. Azad, A. Echols, V. A. Kulyukin, R. Zane and Z. Pantic, "Analysis, Optimization, and Demonstration of a Vehicular Detection System Intended for Dynamic Wireless Charging Applications," in IEEE Transactions on Transportation Electrification, vol. 5, no. 1, pp. 147-161, March 2019.

[3] K. Sasaki and T. Imura, “Combination of Sensorless Energized Section Switching System and Double-LCC for DWPT,” 2020 IEEE PELS Workshop on Emerging Technologies: Wireless Power Transfer(WoW), pp62-67, 2020.

[4] Y. Yamada, T. Imura, and Y. Hori, “A Method for Determining Resonant Elements Considering the Requirements of Double-LCC Circuits in Dynamic Wireless Power Transfer,” 2022 Wireless Power Week (WPW), pp.766-771, 2022.

[5] D. Kobayashi, T. Imura, and Y. Hori, “Real-time coupling coefficient estimation and maximum efficiency control on dynamic wireless power transfer for electric vehicles,” in Proc. IEEE PELS Workshop Emerging Technol., Wireless Power, 2015, pp. 1–6.

[6] X. Hu, Y. Wang, Y. Jiang and X. Dong, “Maximum Efficiency Tracking for Dynamic Wireless Power Transfer System Using LCC Compensation Topology,” 2020 IEEE 4th Conference on Energy Internet and Energy System Integration (EI2), pp1992-1996, 2020.

[7] J. Liu, Z. Liu, and H. Su, " Passivity-Based PI Control for Receiver Side of Dynamic Wireless Charging System in Electric Vehicles," IEEE Transactions on Industrial Electronics, vol. 69, no. 1, pp. 783-794, Jan. 2022.